WangWangBaoShaoZhangYangZhuDeng2014

CrystEngComm

PAPER

View Article Online
View Journal | View Issue

Lateral homoepitaxial growth of graphene†

Cite this: *CrystEngComm*, 2014, **16**, 2593

Hong Wang,[a] Guanzhong Wang,*[a] Pengfei Bao,[a] Zhibin Shao,[a] Xiang Zhang,[b] Shaolin Yang,[a] Wei Zhu[a] and Bingchen Deng[b]

Received 14th October 2013,
Accepted 18th December 2013

DOI: 10.1039/c3ce42072h

www.rsc.org/crystengcomm

In this paper, we present electron diffraction and high-resolution transmission electron microscopy (HRTEM) evidence that graphene can be laterally homoepitaxially grown from homo-seeds. We demonstrate that exfoliated thin graphite flakes and CVD-grown graphene grains can both serve as seed crystals. Raman spectra indicate that the epitaxial graphene is 1–2 layers thick, regardless of seed thickness. A two-step growth procedure is developed to epitaxially synthesize large graphene grains. Lateral homoepitaxial growth makes it a reality to duplicate the structure and increase the size of small high-quality graphene crystals.

1. Introduction

Two-dimensional graphene research has attracted renewed interest in the past few years owing to its outstanding electrical, optical, mechanical and thermal properties.[1–3] Graphene has shown great promise in many applications, such as electronic devices,[4,5] transparent electrodes[6–9] and sensors.[10] Meanwhile, the demand for high-quality graphene is steadily growing. Graphene grown by Chemical Vapor Deposition (CVD) demonstrates the advantage of obtaining large single-crystal samples.[11–14] However, the mobility of CVD-grown single-crystal graphene is still lower than that of exfoliated graphene.[13–17] Epitaxy is a traditional method of growing high-quality crystals for many semiconductor materials. Graphene synthesis by heteroepitaxal methods on silicon carbide[18,19] and transition metals (*e.g.*, Ru(0001),[20,21] Ir(111),[22,23] Pt(111)[24,25] and Ni(111)[26]) has been widely investigated. In the contrary, homoepitaxial growth of graphene has been more challenging. Yan *et al.* reported a layer-by-layer growth of bilayer Bernal graphene *via* the CVD method,[27] which demonstrated vertical homoepitaxial growth of graphene.

Lateral homoepitaxial growth could be more significant in high-quality graphene production. As is well known, mechanically exfoliated graphene has the best lattice structure and exhibits the most superior properties. Unfortunately, the size of the exfoliated sample is quite small. It is of great significance if one can duplicate the structure and increase the size of small high-quality graphene crystals. Some groups reported that graphene can be grown from exfoliated graphene seeds[28–30] or by a two-step CVD method,[31,32] and some of them speculated that the growth may be an epitaxial process, however, the homoepitaxial relationship between the grown graphene layer and exfoliated seeds has never been demonstrated.

Here, we give direct evidence that lateral homoepitaxial growth of graphene can be obtained from small exfoliated thin graphite flakes or CVD-grown graphene seeds. Lateral homoepitaxial growth will not only expand our understanding of the mechanism of graphene growth, but also may pave the way of fabricating large high-quality single-crystal graphene.

2. Experimental

2.1 Graphene growth from exfoliated thin graphite flakes

(a) Preparation of exfoliated graphite flakes on Cu foils. Firstly, multilayer graphite–graphene flakes were deposited on SiO_2/Si substrate by mechanical exfoliation of highly oriented pyrolytic graphite (HOPG). Then, the graphite–graphene flakes were transferred to Cu foils (25 μm thick, 99.8%, Alfa Aesar, #13382, cleaned by diluted acetic acid and acetone before use) using the method proposed by Reina *et al.*[33]

(b) Seeded growth. Graphite flakes on Cu foils were loaded into a quartz tube in a furnace. The temperature was increased to 600 °C with flowing 20 sccm H_2 at a pressure of ~0.3 Torr, then heated to 1025 °C with flowing 300 sccm Ar and 7 sccm H_2 at a total pressure of ~21 Torr to avoid etching of thin graphite. Seeded growth was carried out at that temperature and ~10 Torr pressure with a mixture of 1 sccm CH_4 and 500 sccm H_2. After 1–2 min, the growth was stopped by shutting off H_2 and CH_4 flow, then 1000 sccm Ar was introduced immediately. The sample was first slowly cooled down

[a] *Hefei National Laboratory for Physical Sciences at Microscale, and Department of Physics, University of Science and Technology of China, Hefei, Anhui, 230026, PR China. E-mail: gzwang@ustc.edu.cn*
[b] *School of the Gifted Young, University of Science and Technology of China, Hefei, Anhui, 230026, PR China*

† Electronic supplementary information (ESI) available. See DOI: 10.1039/c3ce42072h

(~0.1 °C s^{-1} under 300 sccm Ar and 4 sccm H_2, ~21 Torr total pressure) to 500 °C and then quickly to room temperature.

2.2 Graphene growth from CVD-synthesized graphene grains

Copper foils were firstly inserted into a quartz tube in the furnace and heated to 1045 °C with flowing 20 sccm H_2 at a pressure of ~0.3 Torr. Then, the temperature was held for 3 h with flowing 300 sccm Ar and 50 sccm H_2 at a total pressure of ~25 Torr. Graphene grains were firstly synthesized with 0.4 sccm CH_4 and 500 sccm H_2 at ~10 Torr total pressure for 12 min. After that, the CH_4 flow was turned off and the Cu foil was annealed under ~21 Torr pressure for 5 min with flowing 300 sccm Ar and 6 sccm H_2. Then, the gases were switched back to 0.4 sccm CH_4 and 500 sccm H_2 (~10 Torr total pressure) for a secondary growth. After another 12 min growth, the sample was cooled using the same method in section 2.1. The time plot of the entire growth process is shown in Fig. S3.†

2.3 Graphene transfer

Copper foils were removed from the Marble's reagent solution ($CuSO_4$: HCl : H_2O = 10 g : 50 ml : 50 ml) while the graphene grains were protected by spin-coated PMMA layers. Then, the PMMA-supported graphene grains were picked up with 300 nm SiO_2/Si substrates or transmission electron microscopy (TEM) grids. Finally, the PMMA layers were removed with acetone. For graphene grains transferred to TEM grids, six to seven drops of acetone were used to dissolve the PMMA layers.

2.4 Characterization

TEM and selected area electron diffraction (SAED) were performed using JEOL JEM-ARM 200F (non-spherical-aberration-corrected TEM mode), JEM-2000 (Fig. 2 and S2†) and JEM-2010F (Fig. 3c). Both transmission electron microscopes were operated at 200 kV. Raman spectra and Raman mapping were recorded at room temperature using Horiba Jobon Yvon micro-Raman spectrometer with laser excitation at 514 nm. All the Raman maps had a pixel size of 0.6 μm along both x and y directions.

3. Results and discussion

The key point of our experiment is that ultrathin graphite flakes were utilized as the growth seeds, which makes it possible to determine their crystal orientations after a high temperature process (as will be discussed later). A sophisticated procedure was used to deposit thin graphite flakes on a catalytic Cu substrate (Fig. 1a). Fig. S1 in the ESI† displays the same flake on SiO_2/Si and Cu substrates. The Raman spectrum demonstrates that the good quality of the thin graphite flake was maintained through the transferring process. After the seeded growth, the thin graphite flake is surrounded with graphene films (Fig. 1b). The size of the newly grown graphene flake can be controlled by the CH_4 feeding time. Other random nucleation can also be found on Cu foils after the

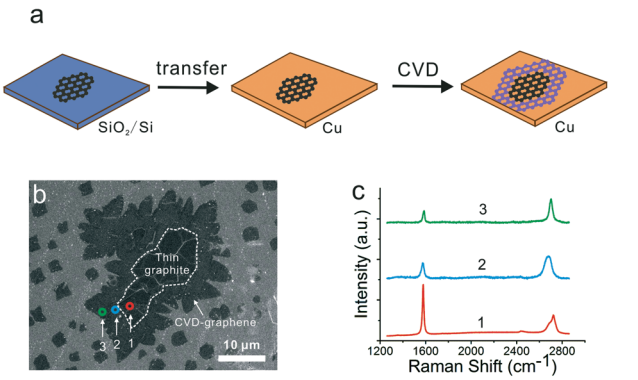

Fig. 1 (a) Schematic illustration of thin graphite transfer from 300 nm SiO_2/Si to a Cu foil substrate, and the seeded growth. (b) SEM image of multilayer graphite flakes surrounded by graphene layers after the CVD growth. (c) Raman spectra of different areas indicated in (b).

CVD process. Raman spectra of the seed and the newly synthesized graphene are given in Fig. 1c, the seed shows typical features of multilayer graphite while its surrounding graphene is 1–2 layers thick.

A thin graphite flake after epitaxial growth was transferred to a TEM grid. Fig. 2a shows its TEM image. As we can see in Fig. 2a, the exfoliated graphite flake was surrounded by thinner films. The thick area on the right was identified as the seed while the thin film on the left was identified as CVD-grown graphene. A distinct boundary can be found between the two areas. SAED was used to characterize crystal orientation of the original exfoliated thin graphite flake and its neighboring deposited graphene. As shown in Fig. S2 (ESI†), after high temperature annealing (1025 °C), slightly thicker graphite seeds obtained by an exfoliation method always become partially or fully non-Bernal stacked. The complicated moiré patterns and SAED patterns suggest relative rotation of consecutive layers within the graphite flake.[34–37] In this case, the crystal orientation relationship between the seed and CVD-grown graphene cannot be well demonstrated. In some selected area with fewer graphene layers, the SAED pattern is less complicated (Fig. 2b) and features a single set of bright hexagonal spots, and exhibits same orientation with the SAED patterns obtained on the CVD deposited areas (Fig. 2c). This suggests that the surrounding graphene was grown epitaxially from the seed.

We further investigated the detailed atomic structure near the epitaxial interface. HRTEM lattice fringe images of the CVD-grown graphene and graphite seed at the two sides of interface are shown in Fig. 2d and g. Due to the wide existence of ripples in 2D graphene, it is difficult to obtain lattice fringe images with a non-aberration-corrected TEM. The lattice fringes of the graphite seed are easily visible (Fig. 2g), while graphene lattice can hardly be resolved from the image (Fig. 2d). However, the fast Fourier transform (FFT) pattern (Fig. 2e) of the selected region in Fig. 2d shows one set of sharp six-fold spots, which exhibit the same orientation with the SAED patterns in Fig. 2b and c. For clarity, mask-filtered

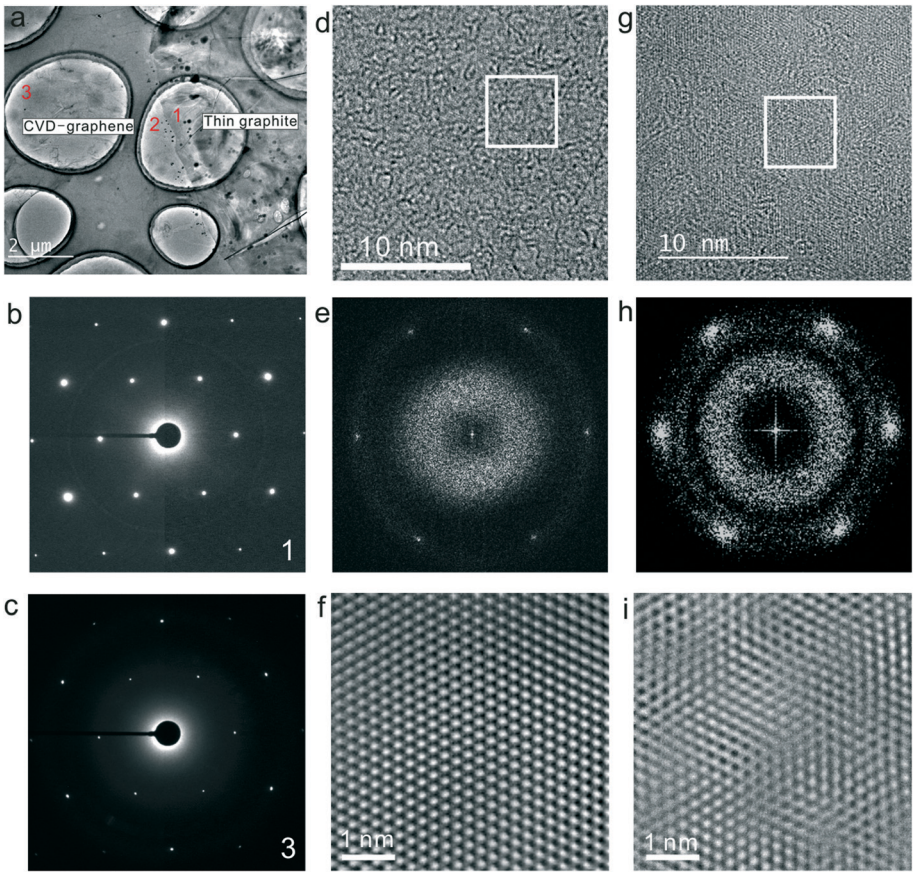

Fig. 2 (a) Low magnification TEM image shows a distinct boundary separating exfoliated thin graphite flake and CVD-grown graphene. (b, c) SAED of the "1" and "3" areas marked in (a), respectively. (d, g) HRTEM image of CVD-grown graphene (the region marked as "2" in panel a) and the exfoliated multilayer graphite flake (the region marked as "1" in panel a). Panel g shows resolvable lattice fringes. (e, h) FFT patterns from white boxed area in panels (d) and (g), respectively. (f, i) Filtered HRTEM images of insets in panels (d) and (g), respectively.

images of Fig. 2d and g are given in Fig. 2f and i, respectively, which show that CVD-grown graphene has the same hexagonal lattice orientation as that of the exfoliated graphite seed. The epitaxial graphene film is mostly 1–2 layers thick under our CVD growth condition, while the exfoliated graphite flake has multiple layers. However, due to the equipment limitations, we cannot tell how the carbon atoms were connected at the thin graphite–graphene interface.

Meanwhile, non-expitaxial growth, revealed by different oriented diffraction spots of the seeds and deposited graphene, has also been observed in the same sample with expitaxial graphene domains. However, it is always not easy to resolve the crystal orientation relationship between the deposited graphene and the seeds, especially for thick seeds. The difficult mainly comes from complicated moiré patterns induced by atomic layers in a graphite seed rotated with each other, which always occurs for a graphite seed experienced high temperature treatment in the CVD process.

On the basis of the findings above, we developed a two-step growth process to epitaxially synthesize large-size single-crystal graphene films. As shown in Fig. S3 (ESI†), graphene grains (which act as the seed) were synthesized on Cu foils with our former proposed method,[12] followed by an Ar/H_2 annealing process at the same temperature. Then CH_4 was introduced for a secondary growth. After the growth, an inner boundary area with the same shape of the grain boundary was observed in each grain by dark-field optical microscopy (Fig. 3a). Optical microscopy images of the transferred sample reveal that additional graphene nucleation occurs in the inner boundary area (Fig. 4a and b). The small grains are usually several micrometers in size. It is suggested that the large grains experienced two-step growth and their sizes were doubled, while many tiny grains developed from new nuclei and left in the inner boundary areas. According to Gao *et al.*,[38] graphene nucleation tends to occur near a step edge due to a lower nucleation barrier, which accounts for the existence of small grains in the inner boundary areas.

To fully characterize the sample crystallinity, large graphene grains were transferred to TEM grids for analysis by SAED. Fig. 3b shows an optical image of a square domain on a TEM grid, in which residual PMMA on graphene helps to show the entire domain clearly. SAED patterns recorded from graphene grown in the first and second stage display the same set of hexagonal diffraction spots without rotation (Fig. 3c), which suggest that the two regions have the same crystal orientation. In other words, the secondary graphene

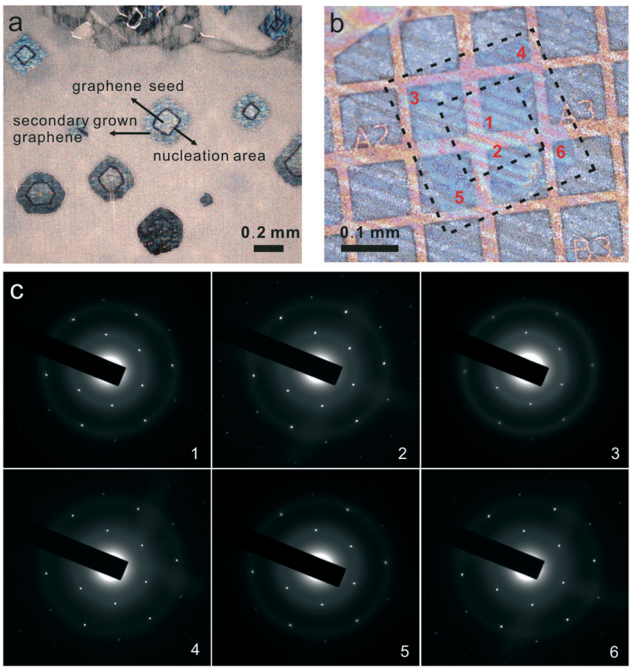

Fig. 3 (a) Dark-field Optical microscopy (OM) image of graphene grains on Cu foils synthesized by a two-step growth method. The color of graphene grains under dark-field OM has apparent contrast with the copper substrate. (b) OM image of a square graphene grain transferred to a Cu TEM grid. The dotted lines represent the seed and epitaxially grown region. (c) SAED taken from different areas of the grain shown in (b), indicating epitaxial growth of the graphene grain.

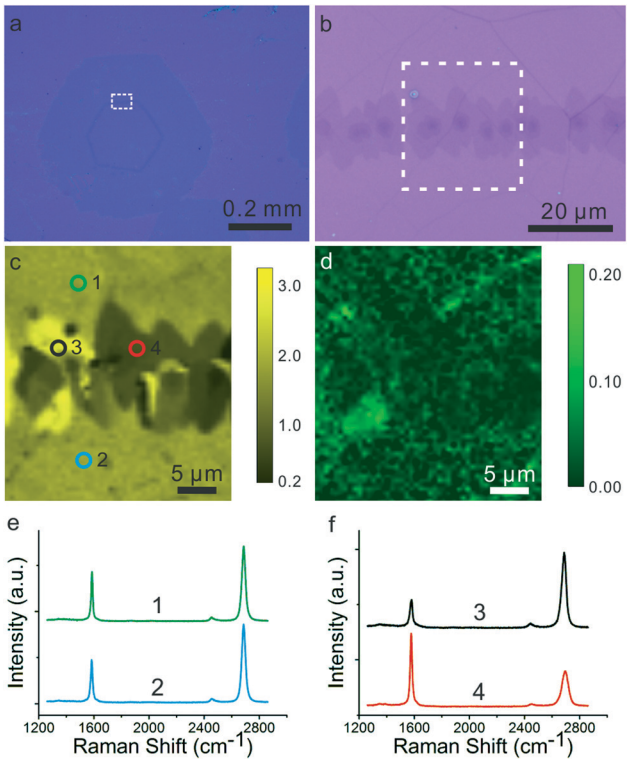

Fig. 4 (a) Low and (b) high magnification OM images of a graphene grain transferred to SiO_2/Si substrate, displaying continuous nucleation along the inner boundary area. (c, d) Raman map of the I_{2D}/I_G (c) and I_D/I_G (d) measured in the area indicated in (b). (e, f) Raman spectra of different areas marked in (c).

grew epitaxially from the primary part. However, the crystallinity of the micro-grains in the inner boundary area is unclear since they can hardly be identified by TEM.

Raman spectroscopy was used to evaluate the uniformity of the graphene films synthesized in different stages. Fig. 4c and d show Raman mapping images of the intensity ratios (I_{2D}/I_G and I_D/I_G) of 2D (~2689 cm^{-1}) and D bands (~1347 cm^{-1}) to G band (~1587 cm^{-1}) near the inner boundary area. The two sides of the inner boundary area display similar color, indicating that the epitaxial film and seeded film are both monolayer with a low defect density ($I_D/I_G < 0.2$ for the scanned area). Fig. 4f displays two distinct Raman spectra of multilayer graphene grains in the inner boundary area: $I_{2D}/I_G < 1$ and the full width at half maximum of the 2D band, FWHM (2D) >45 cm^{-1} for coupled multilayers (red line); $I_{2D}/I_G > 2$ and FWHM (2D) <32 cm^{-1} for decoupled or weakly coupled multilayers (black line).[39]

4. Conclusions

In conclusion, our experiments have shown that exfoliated graphite flakes as well as CVD-synthesized graphene grains can serve as seed crystals for lateral homoepitaxial single-crystal graphene growth. Graphene epitaxial growth from thin exfoliated graphite flakes and CVD-synthesized grains has been suggested by SAED and HRTEM. The experimental results show that the epitaxial graphene is 1–2 layers thick, regardless of seed thickness. Lateral homoepitaxial growth provides a way to duplicate the structure and increase the size of high-quality graphene crystals.

Acknowledgements

We thank Dr Lei Zhou for his help in the preparation of this paper, and Mr Gongpu Li for his assistance in TEM experiments. This work was supported by the National Basic Research Program of China (2011CB921400, 2013CB921800) and the Natural Science Foundation of China (Grant no. 11374280, 50772110), X. Zhang and B. C. Deng acknowledge the support by the Fund for Fostering Talents in Basic Science of the National Natural Science Foundation of China (no. J1103207) and the National Undergraduate Innovative Training Program (201210358003).

Notes and references

1 K. S. Novoselov, A. K. Geim, S. V. Morozov, D. Jiang, Y. Zhang, S. V. Dubonos, I. V. Grigorieva and A. A. Firsov, *Science*, 2004, **306**, 666–669.
2 K. I. Bolotin, K. J. Sikes, Z. Jiang, M. Klima, G. Fudenberg, J. Hone, P. Kim and H. L. Stormer, *Solid State Commun.*, 2008, **146**, 351–355.

3 J. H. Seol, I. Jo, A. L. Moore, L. Lindsay, Z. H. Aitken, M. T. Pettes, X. Li, Z. Yao, R. Huang, D. Broido, N. Mingo, R. S. Ruoff and L. Shi, *Science*, 2010, **328**, 213–216.
4 F. Schwierz, *Nat. Nanotechnol.*, 2010, **5**, 487–496.
5 F. N. Xia, D. B. Farmer, Y. M. Lin and P. Avouris, *Nano Lett.*, 2010, **10**, 715–718.
6 K. S. Kim, Y. Zhao, H. Jang, S. Y. Lee, J. M. Kim, K. S. Kim, J. H. Ahn, P. Kim, J. Y. Choi and B. H. Hong, *Nature*, 2009, **457**, 706–710.
7 S. Bae, H. Kim, Y. Lee, X. Xu, J.-S. Park, Y. Zheng, J. Balakrishnan, T. Lei, H. Ri Kim, Y. I. Song, Y.-J. Kim, K. S. Kim, B. Ozyilmaz, J.-H. Ahn, B. H. Hong and S. Iijima, *Nat. Nanotechnol.*, 2010, **5**, 574–578.
8 X. Zhang, C. Xie, J. Jie, X. Zhang, Y. Wu and W. Zhang, *J. Mater. Chem. A*, 2013, **1**, 6593–6601.
9 Y. Wu, X. Zhang, J. Jie, C. Xie, X. Zhang, B. Sun, Y. Wang and P. Gao, *J. Phys. Chem. C*, 2013, **117**, 11968–11976.
10 F. Schedin, A. K. Geim, S. V. Morozov, E. W. Hill, P. Blake, M. I. Katsnelson and K. S. Novoselov, *Nat. Mater.*, 2007, **6**, 652–655.
11 X. Li, C. W. Magnuson, A. Venugopal, R. M. Tromp, J. B. Hannon, E. M. Vogel, L. Colombo and R. S. Ruoff, *J. Am. Chem. Soc.*, 2011, **133**, 2816–2819.
12 H. Wang, G. Wang, P. Bao, S. Yang, W. Zhu, X. Xie and W.-J. Zhang, *J. Am. Chem. Soc.*, 2012, **134**, 3627–3630.
13 L. Gao, W. Ren, H. Xu, L. Jin, Z. Wang, T. Ma, L.-P. Ma, Z. Zhang, Q. Fu, L.-M. Peng, X. Bao and H.-M. Cheng, *Nat. Commun.*, 2012, **3**, 699.
14 Z. Yan, J. Lin, Z. Peng, Z. Sun, Y. Zhu, L. Li, C. Xiang, E. L. Samuel, C. Kittrell and J. M. Tour, *ACS Nano*, 2012, **6**, 9110–9117.
15 J. Chen, Z. Jin, P. Ma, H. Wang, H. Wang, J. Shi, S. Peng, X. Liu and T. Ye, *Appl. Phys. Lett.*, 2012, **101**, 172107.
16 S. Chen, H. Ji, H. Chou, Q. Li, H. Li, J. W. Suk, R. Piner, L. Liao, W. Cai and R. S. Ruoff, *Adv. Mater.*, 2013, **25**, 2062–2065.
17 A. K. Geim and K. S. Novoselov, *Nat. Mater.*, 2007, **6**, 183–191.
18 C. Berger, Z. M. Song, T. B. Li, X. B. Li, A. Y. Ogbazghi, R. Feng, Z. T. Dai, A. N. Marchenkov, E. H. Conrad, P. N. First and W. A. de Heer, *J. Phys. Chem. B*, 2004, **108**, 19912–19916.
19 A. Ouerghi, A. Kahouli, D. Lucot, M. Portail, L. Travers, J. Gierak, J. Penuelas, P. Jegou, A. Shukla, T. Chassagne and M. Zielinski, *Appl. Phys. Lett.*, 2010, **96**, 191910.
20 S. Marchini, S. Günther and J. Wintterlin, *Phys. Rev. B: Condens. Matter Mater. Phys.*, 2007, **76**, 075429.
21 P. W. Sutter, J.-I. Flege and E. A. Sutter, *Nat. Mater.*, 2008, **7**, 406–411.
22 A. T. N'Diaye, J. Coraux, T. N. Plasa, C. Busse and T. Michely, *New J. Phys.*, 2008, **10**, 043033.
23 I. Pletikosić, M. Kralj, P. Pervan, R. Brako, J. Coraux, A. T. N'Diaye, C. Busse and T. Michely, *Phys. Rev. Lett.*, 2009, **102**, 056808.
24 T. A. Land, T. Michely, R. J. Behm, J. C. Hemminger and G. Comsa, *Surf. Sci.*, 1992, **264**, 261–270.
25 M. Gao, Y. Pan, L. Huang, H. Hu, L. Z. Zhang, H. M. Guo, S. X. Du and H.-J. Gao, *Appl. Phys. Lett.*, 2011, **98**, 033101.
26 J. C. Shelton, H. R. Patil and J. M. Blakely, *Surf. Sci.*, 1974, **43**, 493–520.
27 K. Yan, H. Peng, Y. Zhou, H. Li and Z. Liu, *Nano Lett.*, 2011, **11**, 1106–1110.
28 W. Wu, L. A. Jauregui, Z. Su, Z. Liu, J. Bao, Y. P. Chen and Q. Yu, *Adv. Mater.*, 2011, **23**, 4898–4903.
29 Q. Yu, L. A. Jauregui, W. Wu, R. Colby, J. Tian, Z. Su, H. Cao, Z. Liu, D. Pandey, D. Wei, T. F. Chung, P. Peng, N. P. Guisinger, E. A. Stach, J. Bao, S.-S. Pei and Y. P. Chen, *Nat. Mater.*, 2011, **10**, 443–449.
30 P.-Y. Teng, C.-C. Lu, K. Akiyama-Hasegawa, Y.-C. Lin, C.-H. Yeh, K. Suenaga and P.-W. Chiu, *Nano Lett.*, 2012, **12**, 1379–1384.
31 X. Li, C. W. Magnuson, A. Venugopal, J. An, J. W. Suk, B. Han, M. Borysiak, W. Cai, A. Velamakanni, Y. Zhu, L. Fu, E. M. Vogel, E. Voelkl, L. Colombo and R. S. Ruoff, *Nano Lett.*, 2010, **10**, 4328–4334.
32 K. Yan, D. Wu, H. Peng, L. Jin, Q. Fu, X. Bao and Z. Liu, *Nat. Commun.*, 2012, **3**, 1280.
33 A. Reina, H. Son, L. Jiao, B. Fan, M. S. Dresselhaus, Z. Liu and J. Kong, *J. Phys. Chem. C*, 2008, **112**, 17741–17744.
34 M. Kuwabara, D. R. Clarke and D. A. Smith, *Appl. Phys. Lett.*, 1990, **56**, 2396–2398.
35 J. Xhie, K. Sattler, M. Ge and N. Venkateswaran, *Phys. Rev. B: Condens. Matter Mater. Phys.*, 1993, **47**, 15835–15841.
36 Z. Y. Rong and P. Kuiper, *Phys. Rev. B: Condens. Matter Mater. Phys.*, 1993, **48**, 17427–17431.
37 T. S. Ong and H. Yang, *Carbon*, 2000, **38**, 2077–2085.
38 J. Gao, J. Yip, J. Zhao, B. I. Yakobson and F. Ding, *J. Am. Chem. Soc.*, 2011, **133**, 5009–5015.
39 Z. Luo, T. Yu, J. Shang, Y. Wang, S. Lim, L. Liu, G. G. Gurzadyan, Z. Shen and J. Lin, *Adv. Funct. Mater.*, 2011, **21**, 911–917.